

UDPNet: Unleashing Depth-based Priors for Robust Image Dehazing

Zengyuan Zuo · Junjun Jiang · Gang Wu · Xianming Liu

Received: date / Accepted: date

Abstract Image dehazing has witnessed significant advancements with the development of deep learning models. However, a few methods predominantly focus on single-modal RGB features, neglecting the inherent correlation between scene depth and haze distribution. Even those that jointly optimize depth estimation and image dehazing often suffer from suboptimal performance due to inadequate utilization of accurate depth information. In this paper, we present UDPNet, a general framework that leverages depth-based priors from large-scale pretrained depth estimation model DepthAnything V2 to boost existing image dehazing models. Specifically, our architecture comprises two typical components: the Depth-Guided Attention Module (DGAM) adaptively modulates features via lightweight depth-guided channel attention, and the Depth Prior Fusion Module (DPFM) enables hierarchical fusion of multi-scale depth map features by dual sliding-window multi-head cross-attention mechanism. These modules ensure both computational efficiency and effective integration of depth priors. Moreover, the intrinsic robustness of depth priors empowers the network to dynamically adapt to varying haze densities, illumination conditions, and domain gaps across synthetic and real-world data. Extensive experimental results demonstrate

Zengyuan Zuo
 24s103286@stu.hit.edu.cn

Junjun Jiang
 jiangjunjun@hit.edu.cn

Gang Wu
 gwu@hit.edu.cn

Xianming Liu
 csxm@hit.edu.cn

School of Computer Science and Technology, Harbin Institute of Technology, Harbin 150001, China

the effectiveness of our UDPNet, outperforming the state-of-the-art methods on popular dehazing datasets, such as 0.85 dB PSNR improvement on the SOTS dataset, 1.19 dB on the Haze4K dataset and 1.79 dB PSNR on the NHR dataset. Our proposed solution establishes a new benchmark for depth-aware dehazing across various scenarios. Pretrained models and codes will be released at our project <https://github.com/Harbinzzy/UDPNet>.

1 Introduction

Image dehazing, a fundamental low-level image restoration task, plays an essential preprocessing role in enhancing the reliability of downstream high-level vision systems (*e.g.*, object detection, semantic segmentation). According to the ASM Middleton (1957), the degradation process of hazy images can be mathematically described as:

$$H^c(x, y) = J^c(x, y) \cdot t(x, y) + A^c \cdot (1 - t(x, y)) \quad (1)$$

where (x, y) represents the pixel coordinate, $c \in \{r, g, b\}$ is the color channel, H denotes the hazy image, J denotes the corresponding clear image, A is the atmospheric light. The transmission map is usually modeled as $t(x, y) = e^{-\beta \cdot d(x, y)}$ with the scattering coefficient β and the scene depth $d(x, y)$. It follows from the above equation that the estimation accuracy of the transmission map and atmospheric light is crucial to traditional dehazing methods Berman et al (2018); He et al (2012); Ju et al (2019); Zhao (2021); Zhu et al (2015), which rely on reasonable assumptions or statistical priors (see Fig. 1 (a)). However, the complexity of real-world environments often leads to violations of the underlying priors, thereby reducing

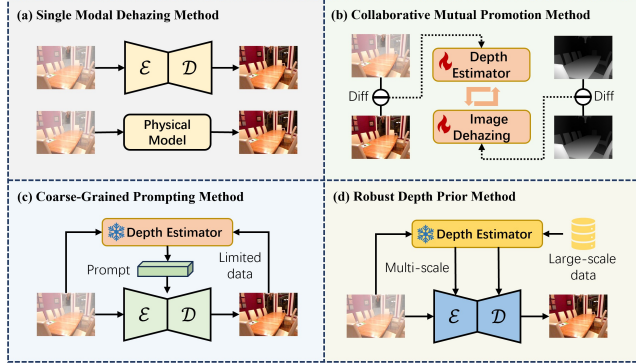


Figure 1 Illustration of Representative Image Dehazing Frameworks. (a) Approaches based on deep learning Cui et al (2023b, 2024a); Dong et al (2020); Guo et al (2022); Hong et al (2020); Jin et al (2025); Liu et al (2021b); Qiu et al (2023); Wu et al (2021); Zamir et al (2022) or physical models Berman et al (2018); He et al (2010, 2012); Ju et al (2019); Zhao (2021); Zhu et al (2015) fail in complex distortions due to idealized assumptions and limited data, resulting in unsatisfactory dehazing outcomes and noticeable artifacts. (b) The collaborative mutual promotion between depth estimation and image dehazing Zhang et al (2024) requires alternate training of two networks, and has lower performance in outdoor and real-world scenarios. (c) The depth-consistent dehazing network Wang et al (2024a) according to the differences fails to make good use of depth information. Although the perception quality has been enhanced, the distortion metric is poor. Both (b) and (c) suffer from the inevitable error in depth estimation. (d) Our UDPNet utilizes the robust and reliable depth estimation model trained on large-scale datasets and effectively integrates it into a multi-scale hierarchical network, achieving excellent generalization.

the robustness of traditional dehazing methods. For instance, He et al. He et al (2010) assumed that at least one color channel has very low intensity in most haze-free patches, which may not hold in bright regions such as the sky or objects with high reflectance, resulting in color distortions. Similarly, priors based on color-line distributions Zhu et al (2015) or contrast assumptions Ju et al (2019) can break down in cases where the scene contains complex textures, non-uniform illumination, or artificial light sources. Moreover, the estimation of atmospheric light can be unreliable in scenes with strong sunlight, multiple scattering, or dense haze, further amplifying the reconstruction error. These limitations highlight the inherent fragility of prior-based dehazing when applied to real-world conditions.

With the advent of deep learning, various variations of Convolutional Neural Networks (CNNs) Cui et al (2023b, 2024a); Dong et al (2020); Hong et al (2020); Wu et al (2021) and Transformers Guo et al (2022); Jin et al (2025); Liu et al (2021b); Qiu et al (2023); Zamir et al (2022) have emerged for single image dehazing by learning the strong statistical regularities. They typically compute a sequence of features from the

single-modal RGB input images and directly reconstruct the clear ones (see Fig. 1 (a)). Such approaches have achieved state-of-the-art results on benchmark datasets by leveraging advanced architectural designs such as multi-scale information fusion Cui et al (2023b, 2024a); Liu et al (2019); Ren et al (2020), multi-stage pipelines, sophisticated variants of convolution Cui et al (2024b); Liu et al (2020); Luo et al (2023), attention mechanisms Cui et al (2024a); Liu et al (2019). Nevertheless, dehazing remains an ill-posed inverse problem in which feature estimation errors can markedly degrade restoration quality. Since RGB observations alone provide incomplete and often ambiguous cues under heavy haze, relying exclusively on them limits the model’s ability to resolve uncertainty and correct erroneous predictions. Inspired by the human visual system’s capacity to integrate and reconcile multisensory information for robust perception, we argue that effective dehazing requires the joint exploitation of complementary modalities (e.g., depth maps, FIR Du et al (2025), NIR Feng et al (2013); Li et al (2025), SAR Zhao et al (2025), semantic maps Jin et al (2023b); Zhang et al (2021)) to enhance robustness and generalization in haze removal. The Atmospheric Scattering Model (ASM) Middleton (1957) further provides a theoretical basis, as haze density is intrinsically correlated with scene depth, suggesting a natural synergy between dehazing and depth estimation. Leveraging depth-based priors can thus supply structural guidance and holistic awareness of haze distribution. Following this insight, several recent works Wang et al (2024a); Zhang et al (2024) integrated depth into dehazing frameworks. For instance, DCMPNet Zhang et al (2024) (see Fig. 1 (b)) incorporated the depth estimation and image dehazing model within a unified framework in a dual-task-driven manner. SelfPromer Wang et al (2024a) (see Fig. 1 (c)) extracted the depth difference features between hazy residuals and clear counterparts as prompts to improve haze removal.

However, there still exist three main issues in practical image dehazing: (1) *The acquired depth information is usually inaccurate.* Prior studies have shown that larger datasets and more powerful models provide richer cues beyond basic labeling. Yet existing depth-based methods, whether relying on pretrained depth estimation models Birk et al (2023) with limited training data or lightweight models trained from scratch Yang and Zhang (2022); Zhang et al (2024), still struggle to cope with complex hazy scenes such as nonhomogeneous, dense, or nighttime haze. (2) *The potential of depth information has not been fully exploited.* Although the difference self-prompt approach Wang et al (2024a) improved perceptual



Figure 2 Previous image dehazing methods often lack robustness to changes in scene conditions. In contrast, our general model effectively restores hazy images under varying illumination, varying scenes, haze distributions, and haze densities. Zoom in for more details.

quality, it still performed poorly on distortion-oriented metrics. Similarly, directly integrating depth features at the tail of a UNet backbone [Zhang et al \(2024\)](#) failed to yield satisfactory results. More recently, PromptHaze [Ye et al \(2025\)](#) adopted a relatively straightforward design by injecting depth prompt features as an additional input, which limited its ability to capture the complex interactions between depth and haze. (3) *A lack of universal high-performing dehazing models for both daytime and nighttime dehazing.* Real-world nighttime haze is further complicated by multiple scattering, uneven illumination, glow, blur, and hidden noise, which make it more challenging than daytime haze. Existing state-of-the-art daytime dehazing methods [Guo et al \(2022\)](#); [Jin et al \(2025\)](#); [Liu et al \(2021b\)](#); [Qiu et al \(2023\)](#); [Zamir et al \(2022\)](#) and nighttime counterparts [Jin et al \(2023a\)](#); [Liu et al \(2023\)](#) are typically developed in isolation, and none can effectively handle both scenarios in a single framework. Thus, developing a universal model that can jointly address daytime haze, nighttime haze, and diverse haze conditions is still an urgent yet unresolved challenge, as illustrated in Fig. 2.

To address these challenges, we turn to the fundamental limitations posed by depth estimation and its integration with visual features in the context of image dehazing. Depth estimation, while a promising cue, is often hindered by inherent inaccuracies and limited generalization across complex hazy scenes (Issue 1). In response, we employ DepthAnything V2 [Yang et al \(2024b\)](#), a state-of-the-art pretrained model, which

offers robust and generalizable depth cues. To fully exploit the potential of depth as a structural prior (Issue 2), we propose two novel modules that effectively integrate depth with visual representations. The Depth-Guided Attention Module (DGAM) adaptively modulates feature maps via depth-informed channel attention, ensuring efficient interaction between depth and image content. Complementing this, the Depth Prior Fusion Module (DPFM) enables hierarchical fusion of multi-scale depth features with visual representations, facilitating richer structural guidance and enhancing robustness in dehazing tasks. This dual-module approach bridges the gap between depth and image representations, providing a unified solution for diverse hazy scenarios.

In recent years, foundation models have profoundly influenced various image restoration tasks. However, to the best of our knowledge, no existing work has attempted to jointly address dehazing, nighttime dehazing, and other image restoration tasks using DepthAnything V2, a model inherently related to haze distribution and global structure priors. This work is motivated by the observation that depth-based priors can enhance robustness and reconstruction quality across various scenarios. In summary, our main contributions are as follows:

- We introduce the large-scale pretrained depth estimation model for image dehazing. The incorporation of powerful priors enables our network to generalize to a wide range of hazy image scenarios.
- We propose a general framework that integrates the depth maps into the multi-scale image dehazing networks. Meanwhile, we propose a depth-based prior fusion strategy that balances effectiveness and computational efficiency.
- Our model, UDPNet, achieves state-of-the-art performance on popular dehazing datasets, exhibiting strong robustness across both daytime/nighttime conditions and synthetic/real-world scenarios, while also demonstrating its potential in other image restoration tasks.

The remainder of this paper is organized as follows. Section 2 reviews existing daytime and nighttime image dehazing methods, with a particular focus on depth-based approaches. Section 3 presents our observations and motivation, along with preliminary experiments for validation. Section 4 details the proposed UDPNet model, and Section 5 presents experimental results across various datasets along with discussions on limitations. Finally, Section 6 concludes the paper.

2 Related Work

2.1 Image Dehazing

Image dehazing methods are typically divided into prior-based, learning-based, and hybrid approaches. Because of its ill-posed nature, prior-based methods rely on the atmospheric scattering model and handcrafted priors, such as the dark channel prior (DCP) He et al (2010), color attenuation prior (CAP) Zhu et al (2015), and BCCR Meng et al (2013), to estimate the transmission map and atmospheric light. While effective under ideal conditions that meet their assumptions, these approaches struggle to generalize in complex haze scenarios. In contrast, learning-based methods leverage data-driven architectures such as CNNs Krizhevsky et al (2012) and Transformers Vaswani et al (2017) to achieve superior dehazing performance. Some early models focus on learning transmission maps Cai et al (2016); Ren et al (2016) or jointly learning transmission maps and atmospheric light Li et al (2021); Pang et al (2018); Zhang and Patel (2018). In parallel, RDN Li et al (2020) and Dehaze-RetinexGAN Wang et al (2025b) embed the Retinex-based decomposition model into the dehazing network to improve generalization ability.

However, these methods are susceptible to cumulative errors arising from inaccurate estimations. To avoid this, more recent works Chen et al (2024); Cui et al (2024b); Liu et al (2019); Wang et al (2021) incorporate hierarchical multi-scale representations, attention mechanisms, large-kernel convolutions, etc, enabling effective dehazing without reliance on the physical model. GridDehazeNet Liu et al (2019) employs a three-stage attention-based multi-scale framework to achieve end-to-end dehazing. EPDN Qu et al (2019), a pioneering framework embedding GAN and the enhancer module, generates perceptually pleasing images with realistic colors and fine details. FFA-Net Qin et al (2020) introduces the feature attention (FA) and attention-based feature fusion (FFA) to effectively integrate information across different levels. Cui et al. Cui et al (2023b, 2024a); Su et al (2025) design the hierarchical multi-input multi-output pure convolutional network to recover image sharpness and textures. C²PNet Zheng et al (2023) and PHATNet Tsai et al (2025) incorporate physics priors into the feature space, enhancing interpretability by aligning feature representations with the hazing process. Dehazer Guo et al (2022), DehazeFormer Song et al (2023) and MB-TaylorFormer Qiu et al (2023) leverage Transformers to model long-range dependencies. Concurrently, with the advancement of data-driven methods in dehazing performance, network complexity has also increased.

To mitigate the reliance on large-scale training data, hybrid approaches Mo et al (2022) have been proposed, which integrate inherent image priors with the representation power of deep neural networks. For example, PGH²Net Su et al (2025) introduces triple priors (*i.e.*, bright channel prior, dark channel prior and histogram equalization prior) to UNet-like architecture for efficient image dehazing. Methods like Dudhane and Murala (2019); Fang et al (2025) utilize transformation of color space (YCbCr) to guide the RGB space. Furthermore, SelfPromer Wang et al (2024a) and PromptHaze Ye et al (2025) explore the fruitful combination of depth-based priors with deep dehazing network.

In addition to these architectural advances, several complementary directions have emerged, including methods for nighttime dehazing Jin et al (2023a); Yan et al (2020), haze image generation approaches Wang et al (2025a); Wu et al (2023) for real-world scenarios, and recent efforts toward universal image restoration Jiang et al (2025). For example, NightHazeFormer Liu et al (2023) integrates dual priors into the transformer decoder, effectively guiding the network to learn abundant prior features. NightHaze Lin et al (2025) introduces a self-prior learning paradigm, leveraging MAE-like representations to improve nighttime dehazing performance. Wang et al. Wang et al (2025a) propose HazeGen and DiffDehaze, a diffusion-based hazing-dehazing pipeline. Together, these efforts broaden the scope of dehazing research and lay a solid foundation for addressing more challenging restoration tasks.

2.2 Depth Priors for Image Dehazing

End-to-end dehazing networks relying solely on RGB features have made significant progress but often struggle with ambiguous scene structures and insufficient depth information constraints. In contrast, dehazing approaches Yang and Zhang (2022); Yang et al (2022); Ye et al (2025) incorporating depth maps offer distinct advantages by leveraging the structure priors embedded in data. The intrinsic physical correlation further highlights the potential. Lee et al. Lee et al (2020) propose a CNN-based simultaneous dehazing and depth estimation network with a shared encoder and multiple decoders. Similarly, Yang et al. Yang and Zhang (2022) and Cheng et al. Cheng and Zhao (2021) propose the depth-aware methods to fuse the depth features to the dehazing network. Due to the absence of accurate depth maps during inference and the possible residual haze remaining, Wang et al. Wang et al (2024a) propose a continuous self-prompting inference strategy, which iteratively refines the dehazing results toward clearer outputs. Furthermore, PromptHaze Ye et al (2025)

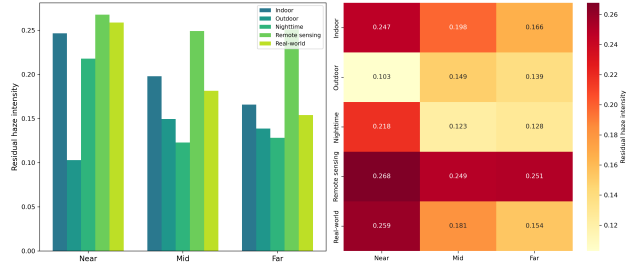


Figure 3 Cross-dataset statistical visualization of residual haze (i.e., haze density) across depth ranges highlighting scene-dependent variations and depth–haze correlations in indoor, outdoor, nighttime, remote sensing, and real-world scenarios.

introduces a dehazing strength factor to achieve a controllable step-by-step dehazing process, thereby alleviating the impact of cumulative errors. Recently, Zhang et al. Zhang et al (2024) integrate lightweight depth estimation model and image dehazing to form a dual-task collaborative optimization. Some novel methods Liu et al (2025); Wu et al (2023); Yang et al (2022); Ye et al (2025) perform online synthesis of realistic hazy images based on depth maps and physical models, facilitating supervised training for real-world dehazing. These innovations inspire us to develop an effective and general dehazing framework that leverages depth priors as guidance. Moreover, our work proposes a general depth map fusion scheme, which is validated through experiments on previous algorithms Cui et al (2023b, 2024a, 2025a,b); Potlapalli et al (2023). In the following sections, we will introduce the detailed design and implementation of our methods.

2.3 DepthAnything vs. Other Depth Estimation Models

DepthAnything Yang et al (2024a) and its successor DepthAnything V2 Yang et al (2024b) represent a significant shift in monocular depth estimation through a precise synthetic and large-scale pseudo-labeled paradigm. Unlike MiDaSv3.1 Birk et al (2023) or AdaBins Bhat et al (2021), which are exclusively trained on manually annotated datasets (e.g., NYU-D Silberman et al (2012), KITTI Geiger et al (2013)), DepthAnything first distilled a high-capacity DINOv2-Giant Oquab et al (2023) teacher model on five high-fidelity synthetic datasets, and then generated pseudo-depth for 62 million in-the-wild real images, effectively bridging the domain gap between synthetic and real-world data distributions. Finally, compact student models (ViTS/B/L/G variants) were trained on these high-quality pseudo-labels. This methodology leads to superior performance in handling thin structures and transparent objects, and significantly improves generalization across

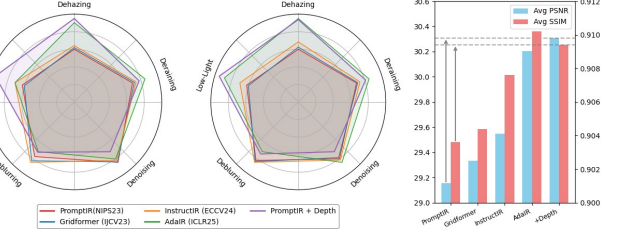


Figure 4 Comparative analysis of the impact of depth map assistance on various image restoration tasks (i.e., dehazing, deraining, denoising, deblurring, and low-light enhancement). Our experiments show that incorporating depth maps yields substantial gains in dehazing and low-light enhancement, demonstrating their potential for both daytime and nighttime dehazing. Moreover, the overall performance achieves state-of-the-art results. Depth maps are generated using DepthAnything-small Yang et al (2024a), and our dehazing network, PromptIR Potlapalli et al (2023), takes both RGB and depth inputs rather than relying solely on RGB features.

complex and challenging scenes. The global depth scene information, coupled with the refined sharpness of depth discontinuities, effectively serves as an auxiliary to image dehazing tasks. Our framework ensures a seamless integration of DepthAnything V2 priors with multi-scale dehazing networks.

3 Preliminary Analysis

In this paper, we propose that the depth prior, often overlooked, is powerful global information inherent to image dehazing. Mathematically, the atmospheric scattering model links the transmission map to depth via

$$t(x, y) = e^{-\beta d(x, y)}. \quad (2)$$

It suggests that deeper regions should appear more heavily degraded. However, in practice this monotonic trend does not always hold across different scenes. To better understand this discrepancy, we analyze the relationship between depth and residual haze, where residual haze is defined as the absolute difference between the hazy input and its corresponding clear image. Specifically, for each dataset we compute a residual haze map, partition the normalized depth into three equal bins (Near, Mid, Far), and calculate the average residual haze intensity within each bin. Fig. 3 presents a cross-dataset statistical analysis. Interestingly, the trends vary significantly across scene categories. Outdoor datasets exhibit stronger haze density in distant regions, which is consistent with physical scattering intuition, whereas indoor datasets show stronger residuals at near distances. Nighttime datasets present different residuals, reflecting the compounded degradations from haze and

illumination. Remote sensing scenes reveal consistently strong haze density across all depths, while real-world datasets demonstrate a mixed trend. These observations highlight that the relationship between depth and haze density is scene-dependent, emphasizing the need to incorporate depth priors for adaptive dehazing, rather than relying on handcrafted priors or rigid physical formula-based constraints.

Meanwhile, we further argue that depth estimation models inherently have the capacity to jointly handle dehazing and low-light enhancement, and this capacity can be further enhanced through elaborate design. In all-in-one image restoration, a single network is expected to address diverse degradations and adaptively decide how to restore the input. Depth information provides valuable guidance, particularly for dehazing and low-light scenarios, by separating foreground from background and enabling more accurate restoration across varying depths. This improves robustness in complex real-world conditions. To validate the effectiveness of our proposed method, we perform preliminary experiments for verification. We experiment with a dedicated all-in-one image restoration network [Potlapalli et al \(2023\)](#) evaluating on the five-degradation scenarios [Jiang et al \(2025\)](#) (modifying the original RGB input by concatenating it with depth maps extracted by DepthAnything-small [Yang et al \(2024a\)](#)). The results are presented in Fig. 4. It can be seen that the average PSNR achieves state-of-the-art performance, with particularly significant improvements on the dehazing and low-light enhancement tasks. This indicates that the depth maps extracted by DepthAnything inherently contribute to both daytime and nighttime image dehazing. Additionally, the depth-based approach shows significant potential for enhancing performance in other image restoration tasks, deserving further exploration.

4 Methodology

In this section, we introduce our proposed depth-based framework, as illustrated in Fig. 4. We first present an overall pipeline of our UDPNet. We then delineate details of our designs: the Depth-Guided Attention Module (detailed in Sec. 4.2.1) and the Depth Prior Fusion Module (detailed in Sec. 4.2.2). The loss functions are introduced in the final part.

4.1 Overall Architecture

In image dehazing, depth information has proven to be a valuable cue for recovering structural details and improving robustness, especially in complex hazy

environments. However, traditional methods often struggle to fully exploit depth priors due to challenges in accurately estimating depth and integrating it effectively with image features. Motivated by this, we aim to integrate depth-based priors into a U-shaped convolutional neural network (CNN) backbone for haze removal. Our approach leverages a pretrained depth estimation model, DepthAnything V2, to generate robust depth maps, which are then used to guide the feature extraction process, enhancing the network’s ability to capture geometric and structural information. By incorporating these priors into an encoder-decoder architecture, we ensure that both high-level and low-level features are effectively utilized, with particular attention to how depth information can aid in early-stage feature extraction.

Specifically, the network is established by incorporating depth-based priors with a U-shaped CNN-based backbone for haze removal. Both the encoder and decoder networks comprise three scales, efficiently learning hierarchical representations. Specifically, given any degraded image $\mathbf{I} \in \mathbb{R}^{3 \times H \times W}$, UDPNet first leverages a frozen DepthAnything V2 to generate robust depth maps with the dimensions of $1 \times H \times W$, where $H \times W$ represents spatial locations. The input image and corresponding depth map are processed by the Depth-Guided Attention Module (DGAM), which adapts the features based on depth information. The resulting features are then passed through an asymmetric encoder-decoder structure.

Each stage of the encoder includes a Depth Prior Fusion Module (DPFM), designed to better integrate depth priors with the visual features. To ensure effective integration, this module is applied in each encoder scale, as depth map information is most beneficial for capturing geometric cues and structural details during the early stages of feature extraction. Introducing the module in the decoder would inject low-frequency information from the depth map into the high-frequency image restoration process, potentially hindering fine-grained detail restoration.

Next, the depth-enhanced features are passed through a three-scale decoder, progressively restoring high-resolution features. During training, a multi-output strategy is employed, where low-resolution clean images are predicted using 3×3 convolutions and image-level skip connections. For brevity, Fig. 5(a) only shows the top-level image skip connection. Although our approach can be applied to various dehazing baselines, we demonstrate the framework on FSNet [Cui et al \(2023b\)](#) for clarity.

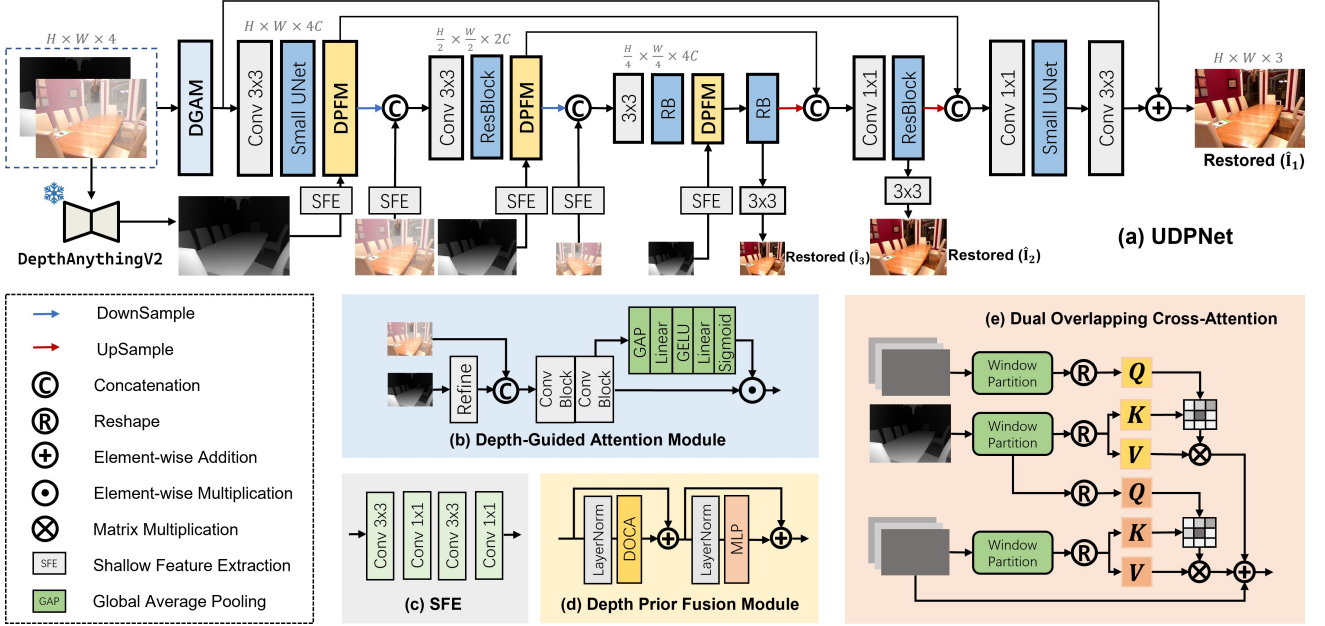


Figure 5 The architecture of our proposed UDPNet (a) is inspired by the symmetric hierarchical encoder-decoder design Cui et al (2023b). UDPNet mainly comprises two organically integrated sub-modules, *i.e.*, DGAM (b) and DPFM (d). DGAM focuses on channel-level fusion between depth-based priors and the input image. DPFM incorporates a multi-scale, multi-head cross-attention mechanism with overlapping windows and dual attention pathways at the spatial level. This design enables UDPNet to act as a general paradigm that leverages depth information to boost existing dehazing models, achieving a trade-off between efficiency and effectiveness.

4.2 Depth Priors Fusion

Effective image dehazing requires not only removal of haze but also faithful recovery of underlying scene structures, spatial consistency, and depth-aware contrasts. While RGB images provide rich color information, they often lack sufficient cues to resolve structural ambiguities, especially in complex haze conditions. Depth priors, capturing geometric layouts and relative distances within a scene, offer complementary information that can guide the network toward more accurate restoration. However, existing methods either rely on simple concatenation of depth maps with image features or apply simple integration strategies, which fail to fully exploit the rich structural knowledge embedded in depth cues. Motivated by this, we aim to systematically incorporate depth priors from a large-scale pretrained model into the dehazing pipeline, enhancing both fidelity and generalization across diverse haze scenarios.

Depth priors provide essential cues for recovering scene structures, depth-aware contrasts, and spatial consistency in degraded images. As a large-scale foundation model trained on diverse image distributions, DepthAnything V2 offers rich geometric knowledge to guide restoration. Leveraging its understanding of spatial layouts and depth relationships, our method incorporates depth-based priors to enhance fidelity and

generalizability. We design two modules to integrate these depth cues into the conventional dehazing pipeline.

4.2.1 Depth-Guided Attention Module

Given a hazy input image $\mathbf{I} \in \mathbb{R}^{3 \times H \times W}$ concatenated with its estimated depth map $\mathbf{D} \in \mathbb{R}^{1 \times H \times W}$, we first refine the depth map using a refinement module to suppress noise and enhance geometric cues. The refinement is implemented as a three-layer convolutional network with ReLU activations:

$$\hat{\mathbf{D}} = \text{Refinement}(\mathbf{D}), \quad (3)$$

where $\hat{\mathbf{D}}$ denotes the optimized depth map.

The refined depth map is concatenated with the RGB image and fed into the subsequent module to extract depth-aware features. We first employ a 3×3 convolution followed by instance normalization and GELU activation to process the concatenated RGB-D input and produce intermediate feature representations. To further enhance feature discrimination, a depth-guided attention mechanism is applied. This module captures global context through adaptive average pooling, generates channel-wise attention weights via two fully connected layers with a GELU nonlinearity, and applies a sigmoid activation. The resulting attention weights are then used to reweight the input features, thereby emphasizing informative

channels and suppressing less relevant ones. Formally, the process can be expressed as

$$\mathbf{F}_{\text{DGAM}} = [\mathbf{I}, \hat{\mathbf{D}}] \odot \sigma(\text{FC}_2(\text{GELU}(\text{FC}_1(\text{GAP}(\mathbf{F}_{\text{conv}})))), \quad (4)$$

where $[\cdot, \cdot]$ is a concatenation operator, \odot denotes element-wise multiplication, GAP is global average pooling, FC_1 and FC_2 are fully connected layers, and σ is the sigmoid activation. By integrating the refined depth map and RGB image through this DGAM, as depicted in Fig. 5(b), the network obtains depth-aware shallow features that benefit subsequent restoration stages. The objective experimental results validate that the proposed DGAM is more effective than a simple concatenation strategy. As detailed in Section 5.4, employing DGAM yields a performance gain on the Haze4K dataset compared to naive feature stacking, demonstrating the advantage of adaptive, depth-guided channel attention.

4.2.2 Depth Prior Fusion Module

The representations encoded in shallow and deep features differ substantially, as they correspond to entirely different receptive fields. This disparity makes it essential to unleash depth priors across multiple feature scales. Inspired by SwinIR Liang et al (2021), HAT Chen et al (2023) and Restormer Zamir et al (2022), we propose a depth prior fusion module (DPFM) to inject estimated depth priors into the multi-scale restoration backbone via a dual cross-attention mechanism defined on overlapping local windows, as shown in Fig. 5(d). Given an intermediate feature map $\mathbf{X} \in \mathbb{R}^{H \times W \times C}$ and a single-channel depth prior $\mathbf{D} \in \mathbb{R}^{H \times W \times 1}$, the depth map is first projected by shallow feature extract to produce depth map features $\mathbf{F}_D \in \mathbb{R}^{H \times W \times C}$. Both \mathbf{X} and \mathbf{F}_D are partitioned into local windows of size $M \times M$ with overlap ratio r (so the effective overlap-window side length is $M_{\text{ov}} = (1+r) \times M$). Zero-padding is first applied to make H and W divisible by M . Queries are then partitioned into non-overlapping windows of size $M \times M$, while keys and values are unfolded from larger overlapping windows of size $M_{\text{ov}} \times M_{\text{ov}}$. This overlap allows each query window to incorporate neighboring context at a controllable cost, thereby propagating geometric cues across adjacent regions while keeping the computation tractable.

Within each local window, we instantiate two complementary cross-attention branches. The depth-guided branch where depth features act as queries and image features provide keys and values, which emphasizes geometric constraints and guides the restoration with

structural priors. The feature-guided branch where image features act as queries and depth features provide keys and values, which enhances the consistency of fine image details with depth information. Together, these two branches form an interaction mechanism that jointly exploits depth and image cues. For a window w (vectorized to $\mathbb{R}^{M^2 \times C}$), let h be the number of heads and $d = C/h$ the per-head dimension; denote by B a learnable relative-position bias. The two branches are written as

$$\text{Attn}_{D \rightarrow X} = \text{Softmax} \left(\frac{Q_D K_X^\top}{\sqrt{d}} + B \right) V_X, \quad (5)$$

$$\text{Attn}_{X \rightarrow D} = \text{Softmax} \left(\frac{Q_X K_D^\top}{\sqrt{d}} + B \right) V_D, \quad (6)$$

with

$$Q_D = \mathbf{F}_{D,w} W_Q^D, \quad K_X = \mathbf{X}_w W_K^X, \quad V_X = \mathbf{X}_w W_V^X,$$

and analogously Q_X, K_D, V_D for the other branch. The window output aggregates both branches with a residual connection:

$$\mathbf{Y}_w = \text{Attn}_{D \rightarrow X} + \text{Attn}_{X \rightarrow D} + \mathbf{X}_w. \quad (7)$$

All window outputs are merged to the full spatial resolution and passed through a pointwise feed-forward network (FFN) with LayerNorm and residual connections to produce the fused feature $\mathbf{Y} \in \mathbb{R}^{H \times W \times C}$, which can be formulated as

$$\mathbf{Y} = \text{DOCA}(\text{LN}(\mathbf{X})) + \mathbf{X}, \quad \mathbf{Y} = \text{MLP}(\text{LN}(\mathbf{Y})) + \mathbf{Y}. \quad (8)$$

In practice, a learnable relative-position bias is introduced to encode spatial priors. Compared to global cross-attention with quadratic cost $\mathcal{O}((HW)^2)$, the window overlapping design yields complexity $\mathcal{O}(HW \cdot M \cdot M_{\text{ov}})$, since each M^2 query interacts with M_{ov}^2 key/value tokens. Although slightly higher than standard non-overlapping window cross attention ($\mathcal{O}(HW \cdot M^2)$), the complexity remains linear in the number of pixels HW and quadratic only in the local window sizes, thus available for high-resolution image restoration. Furthermore, we insert DPFM blocks at multiple encoder stages, allowing depth-aware priors to be progressively injected into the backbone. This hierarchical design enhances geometric consistency and structural fidelity in the restored images, fusing the multi-scale depth information at negligible extra computational cost. The ablation results in Section 5.4 indicate that inserting the DPFM within the encoder stages is more beneficial than placing it in the decoder. This is attributed to

the fact that depth priors provide strong structural and geometric cues that are most effective when integrated during the early stages of feature extraction, providing better guidance for subsequent hierarchical processing. Furthermore, the spatial cross-attention mechanism in DPFM proves particularly effective, contributing significantly to the overall state-of-the-art performance achieved on Haze4K.

4.3 Loss Functions

Following the Cui et al. [Cui et al \(2023b, 2024a\)](#), we employ multi-scale dual-domain loss to train our UDPNet. The spatial and spectral \mathcal{L}_1 loss are given by:

$$\mathcal{L}_{\text{spatial}} = \sum_{i=1}^3 \frac{1}{P_i} \|\hat{\mathbf{I}}_i - \mathbf{Y}_i\|_1, \quad (9)$$

$$\mathcal{L}_{\text{frequency}} = \sum_{i=1}^3 \frac{1}{S_i} \left\| \left[\mathcal{R}(\hat{\mathbf{I}}_i), \mathcal{I}(\hat{\mathbf{I}}_i) \right] - \left[\mathcal{R}(\mathbf{Y}_i), \mathcal{I}(\mathbf{Y}_i) \right] \right\|_1, \quad (10)$$

where i denotes the index corresponding to the multiple output branches illustrated in Fig. 5. $\hat{\mathbf{I}}$ represents the restored image, while \mathbf{Y} denotes the ground truth. The P and S correspond to the total elements for normalization. The notation $[\cdot, \cdot]$ is a concatenation operator, and \mathcal{R} and \mathcal{I} represent the real and imaginary parts obtained through the fast Fourier transform (FFT). The overall loss can be expressed as:

$$\mathcal{L}_{\text{total}} = \mathcal{L}_{\text{spatial}} + \lambda \mathcal{L}_{\text{frequency}}, \quad (11)$$

the balancing hyper-parameter λ is empirically set to 0.1. The parameters of DepthAnything V2 are frozen during the training stage.

4.4 Remarks

Most existing depth-aware dehazing methods adopt simplistic strategies such as directly concatenating depth and RGB inputs or rely on complex auxiliary schemes like joint training with depth estimators or prompt injection. These methods either fail to effectively leverage the structural depth information or introduce additional training complexity, limiting their practical impact. For example, concatenating depth with RGB features at the input stage often results in biasing the network towards low-frequency cues, which diminishes the restoration of high-frequency details.

Similarly, approaches that use auxiliary depth estimators or prompt injection schemes increase optimization complexity without guaranteeing meaningful integration of depth features with the image content.

In contrast, our framework systematically integrates depth priors through two novel modules: the Depth-Guided Attention Module (DGAM) and the Depth Prior Fusion Module (DPFM). DGAM modulates feature representations adaptively based on depth-driven channel attention, thereby ensuring that structural depth cues are enhanced without compromising high-frequency details. The DPFM, on the other hand, performs multi-scale fusion of depth features with visual representations, enabling the network to maintain spatial consistency and geometric awareness across different layers of feature extraction. This approach addresses the fundamental gap in previous methods, effectively combining depth priors with visual information and preserving both structural integrity and fine details.

Experimental results confirm that our approach outperforms existing methods, particularly in dense and nighttime haze conditions, where traditional RGB-based networks often struggle due to the lack of structural cues. The fusion of depth priors not only improves the visual quality of the restored images but also enhances robustness across varying haze intensities and environments. However, it should be noted that the performance of our method is sensitive to the quality of the depth prior, and extreme degradation variations may reduce the effectiveness of depth-based guidance. Nevertheless, our framework still allows for adaptation to other image restoration tasks, such as deblurring and low-light enhancement, which highlights the broader potential of our design in advancing universal image restoration techniques.

5 Experiments

In this section, we conduct extensive experiments to evaluate the effectiveness and generalization of our proposed UDPNet framework. We first introduce the datasets, metrics, and implementation details. Then we perform quantitative and qualitative assessments of the results produced by the proposed UDPNet and other state-of-the-art methods. In the tables, baseline results are marked in blue for clarity. The best and second-best results are highlighted in boldface and underlined, respectively.

Table 1 Summary of datasets used for training and evaluation.

Dataset	Type	Scale / Characteristics	Usage
RESIDE Li et al (2018)	Synthetic	ITS (indoor), OTS (outdoor), SOTS (test, indoor/outdoor)	Train (ITS/OTS), Eval (SOTS)
Haze4K Liu et al (2021a)	Synthetic	4000 paired images, more realistic haze synthesis	Indoor & Outdoor
NH-HAZE Ancuti et al (2020)	Real-world	55 paired hazy/clear images, non-homogeneous haze	Real-world dehazing
Dense-Haze Ancuti et al (2019)	Real-world	55 paired hazy/clear images, homogeneous & dense haze	Real-world dehazing
NHR Zhang et al (2020)	Synthetic	16,146 train pairs, 1,794 test pairs	Nighttime dehazing
GTA5 Yan et al (2020)	Synthetic	Large-scale, game-engine rendered	Nighttime dehazing
SateHaze1k Huang et al (2020)	Synthetic	1,200 hazy/clear pairs, satellite imagery	Remote sensing image dehazing
RESIDE Li et al (2018)	Synthetic	OTS & SOTS-outdoor	Dehazing (all-in-one task)
Rain100L Yang et al (2019)	Synthetic	100 training & 100 testing images	Deraining (all-in-one task)
BSD400 Martin et al (2001)	Real-world	400 images from Berkeley segmentation	Denoising (all-in-one task)
WED Ma et al (2016)	Real-world	4,744 high-quality natural images	Denoising (all-in-one task)
GoPro Nah et al (2017)	Real-world	3,214 blurry/clear pairs from GoPro videos	Deblurring (all-in-one task)
LOL-v1 Wei et al (2018)	Real-world	500 low/normal-light pairs	Low-light enhancement (all-in-one task)

5.1 Datasets and Metrics

Datasets. To comprehensively validate the capabilities of the proposed UDPNet, we conduct an evaluation across diverse dehazing benchmarks, as presented in Table 1. For daytime scenes, we employ both synthetic and real-world datasets. The synthetic benchmarks include RESIDE [Li et al \(2018\)](#), which consists of an indoor training set (ITS), an outdoor training set (OTS) and a synthetic objective test set (SOTS), and a more realistic dataset Haze4K [Liu et al \(2021a\)](#). We train separate models on ITS and OTS using a batch size of 6 and an initial learning rate of 4×10^{-4} , and evaluate them on SOTS-Indoor and SOTS-Outdoor, respectively. We further train our network on Haze4K under identical settings. For real-world evaluation, we test on NH-HAZE [Ancuti et al \(2020\)](#) and Dense-Haze [Ancuti et al \(2019\)](#), each containing 55 paired hazy and clear images. NH-HAZE features non-homogeneous haze, while Dense-Haze features homogeneous and dense haze. In these experiments, we set the batch size to 2, the initial learning rate to 2×10^{-4} , and use patch crops of size 800×1184 following the previous method [Cui et al \(2024a\)](#) and patch crops of size 600×800 following the previous method [Cui et al \(2023b\)](#). Due to GPU memory constraints, we only incorporate the DGAM in the real-world experiments. For nighttime dehazing, we leverage two nighttime dehazing datasets (*i.e.*, NHR [Zhang et al \(2020\)](#), which provides 16,146 training pairs and 1,794 test pairs with a batch size of 6, and GTA5 [Yan et al \(2020\)](#)). In addition, we evaluate our approach on the remote sensing dataset SateHaze1k [Huang et al \(2020\)](#), given the critical role of image dehazing in remote sensing tasks. In addition to single image dehazing, we evaluate the proposed UDP (Unleashing Depth-based Priors) paradigm in all-in-one settings (*i.e.*, five-task configurations [Jiang et al \(2025\)](#)), thereby demonstrating the robustness of our proposed paradigm. The task settings follow AdaIR [Cui et al \(2025b\)](#) (dehazing on SOTS [Li et al \(2018\)](#), deraining on Rain100L [Yang et al \(2019\)](#), denoising on

BSD400 [Martin et al \(2001\)](#) and WED [Ma et al \(2016\)](#), deblurring on GoPro [Nah et al \(2017\)](#), and low-light enhancement on LOL-v1 [Wei et al \(2018\)](#)).

Evaluation Metrics. Across all datasets, we report Peak Signal-to-Noise Ratio (PSNR) and Structural Similarity Index (SSIM) [Wang et al \(2004\)](#) to quantitatively assess dehazing quality. Higher values in both metrics indicate superior restoration quality. For consistency and comparability, we calculate metrics based on identical implementation employed in prior studies [Cui et al \(2024a, 2025b\)](#). On the real-world datasets [Ancuti et al \(2019, 2020\)](#), we further evaluate perceptual similarity using LPIPS [Zhang et al \(2018\)](#), where lower scores indicate better perceptual quality.

5.2 Implementation Details

Our framework is implemented using PyTorch [Paszke \(2019\)](#) and trained on two NVIDIA RTX 3090 GPUs. Following the previous methods [Cui et al \(2023b\); Guo et al \(2022\)](#), each patch is randomly flipped horizontally for data augmentation with a probability of 0.5. The initial learning rate is gradually reduced to 1e-6 with the cosine annealing [Loshchilov and Hutter \(2016\)](#). Adam ($\beta_1 = 0.9$, $\beta_2 = 0.999$) is used for training. Unless specified otherwise, patch size of 256×256 is adopted. We adopt the FSNet [Cui et al \(2023b\)](#), ConvIR [Cui et al \(2024a\)](#), and PoolNet [Cui et al \(2025a\)](#) as our baseline to validate the proposed UDPNet. We follow their original training configurations to ensure a fair comparison. The entire training process lasted for a total of 1000 epochs on the Haze4K, ITS and SateHaze1k datasets, 50 epochs on the OTS dataset, 300 epochs on the NHR dataset, 2000 epochs on the GTA5 dataset, and 5000 epochs on the real-world datasets. For universal image restoration, we follow the settings in [Cui et al \(2025b\)](#). The model is trained for 150 epochs with a batch size of 6. We adopt the L1 loss as the sole optimization objective, and training samples are randomly cropped into patches of size 128×128 .



Figure 6 Image dehazing comparisons on the SOTS-indoor [Li et al \(2018\)](#) dataset. Please zoom in on screen for a better view.



Figure 7 Image dehazing comparisons on the SOTS-outdoor [Li et al \(2018\)](#) dataset. Please zoom in on screen for a better view.

Table 2 Quantitative comparison on the SOTS-Indoor and SOTS-Outdoor datasets [Li et al \(2018\)](#).

Method	Venue	SOTS-Indoor		SOTS-Outdoor	
		PSNR↑	SSIM↑	PSNR↑	SSIM↑
DCP He et al (2010)	TPAMI'10	16.61	0.855	19.14	0.861
GridDehazeNet Liu et al (2019)	CVPR'19	32.16	0.984	30.86	0.982
MSBDN Dong et al (2020)	CVPR'20	33.67	0.985	33.48	0.982
FFA-Net Qin et al (2020)	AAAI'20	36.39	0.989	33.57	0.984
AECR-Net Wu et al (2021)	CVPR'21	37.17	0.990	-	-
MAXIM-2S Tu et al (2022)	CVPR'22	38.11	0.991	34.19	0.985
DeHamer Guo et al (2022)	CVPR'22	36.63	0.988	35.18	0.986
PMNet Ye et al (2022)	ECCV'22	38.41	0.990	34.74	0.985
DehazeFormer-L Song et al (2023)	TIP'23	40.05	0.996	-	-
FSNet Cui et al (2023b)	TPAMI'23	42.45	0.997	40.40	0.997
MB-TaylorFormer-L Qiu et al (2023)	ICCV'23	42.64	0.994	38.09	0.991
FocalNet Cui et al (2023a)	ICCV'23	40.82	0.996	37.71	0.995
C ² PNet Zheng et al (2023)	CVPR'23	42.56	0.995	36.68	0.990
DEA-Net-CR Chen et al (2024)	TIP'24	41.31	0.995	36.59	0.990
DCMPNet Zhang et al (2024)	CVPR'24	42.18	0.997	36.56	0.993
D ⁴ ↑ [†] Yang et al (2024c)	IJCV'24	25.79	0.937	26.30	0.960
GridFormer Wang et al (2024c)	IJCV'24	42.34	0.994	-	-
ConvIR-B Cui et al (2024a)	TPAMI'24	42.72	0.997	39.42	0.996
SFMN Shen et al (2025)	TIP'25	41.44	0.995	37.72	0.991
PoolNet-B Cui et al (2025a)	TIP'25	42.01	0.997	-	-
PGH ² Net Su et al (2025)	AAAI'25	41.70	0.996	37.52	0.989
MB-TaylorFormerV2-L Jin et al (2025)	TPAMI'25	42.84	0.995	39.25	0.992
ConvIR + UDP	Ours	43.12	0.997	40.32	0.996
FSNet + UDP	Ours	43.30	0.997	40.53	0.997

† Denotes the unpaired dehazing method.

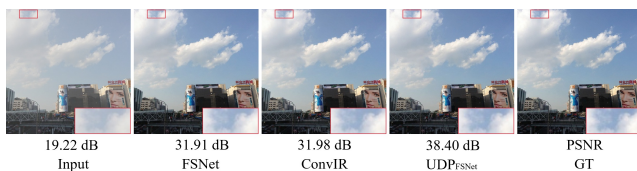


Figure 8 Image dehazing comparisons on the Haze4K [Liu et al \(2021a\)](#) dataset.

Table 3 Quantitative results on the Haze4K [Liu et al \(2021a\)](#) dataset.

Method	PSNR↑	SSIM↑
DehazeNet Cai et al (2016)	19.12	0.84
GridDehazeNet Liu et al (2019)	23.29	0.93
MSBDN Dong et al (2020)	22.99	0.85
FFA-Net Qin et al (2020)	26.96	0.95
DMT-Net Liu et al (2021a)	28.53	0.96
PMNet Ye et al (2022)	33.49	0.98
MB-TaylorFormer-L Qiu et al (2023)	34.47	0.99
FSNet Cui et al (2023b)	34.12	0.99
GridFormer Wang et al (2024c)	33.27	0.99
ConvIR-B Cui et al (2024a)	34.15	0.99
DEA-Net-CR Chen et al (2024)	34.25	0.99
MB-TaylorFormerV2-B Jin et al (2025)	34.92	0.99
ConvIR + UDP (Ours)	34.82	0.99
FSNet + UDP (Ours)	35.31	0.99

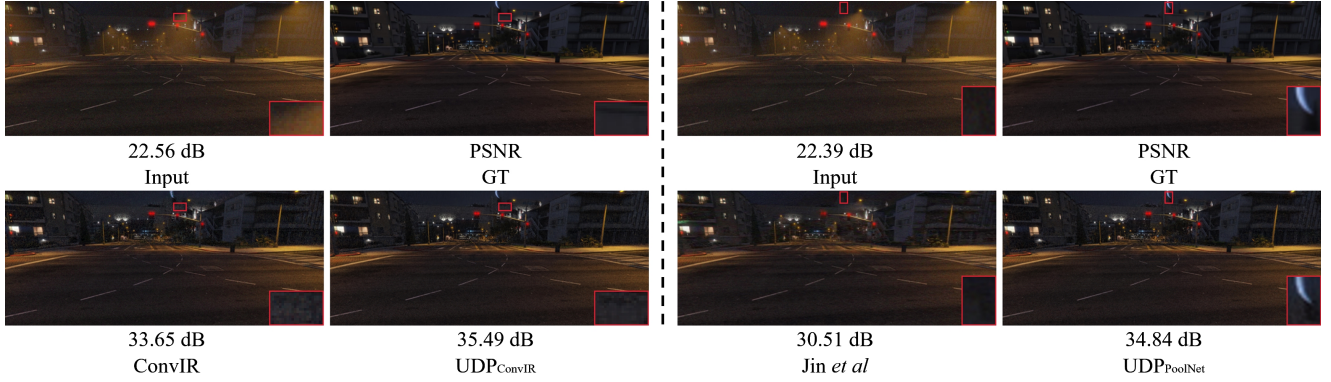
5.3 Comparisons with SOTA Methods

We first present a comprehensive comparison with recent state-of-the-art approaches on the SOTS dataset [Li et al \(2018\)](#) in Table 2. As shown, our proposed methods consistently achieve superior performance across both datasets. In particular, ConvIR + UDP obtains a remarkable PSNR of 43.12 dB on SOTS-Indoor, surpassing the previous best ConvIR-B [Cui et al \(2024a\)](#) and MB-TaylorFormerV2-L [Jin et al \(2025\)](#) by 0.40 dB and 0.28 dB, respectively. On the SOTS-Outdoor dataset, it also achieves a competitive 40.32 dB PSNR, outperforming most recent models such as C²PNet [Zheng et al \(2023\)](#), and DEA-Net [Chen et al \(2024\)](#). More importantly, our FSNet + UDP further pushes the performance boundary, setting a new

Table 4 Quantitative results on the GTA5 [Yan et al \(2020\)](#) dataset.

Method	GS [†] Li et al (2015)	MRP [†] Zhang et al (2017)	Ancuti et al [†] Ancuti et al (2016)	Yan et al [†] Yan et al (2020)	CycleGAN Zhu et al (2017)	Jin et al [†] Jin et al (2023a)	ConvIR-B Cui et al (2024a)	PoolNet-B Cui et al (2025a)	PoolNet + UDP (Ours)	ConvIR + UDP (Ours)
PSNR [†]	21.02	20.92	20.59	27.00	21.75	30.38	31.83	31.53	32.78	33.12
SSIM [†]	0.639	0.646	0.623	0.850	0.696	0.904	0.921	0.921	0.930	0.933

[†] Denotes methods that are specially designed for nighttime image dehazing.

**Figure 9** Nighttime image dehazing comparisons on the GTA5 [Yan et al \(2020\)](#) dataset.**Table 5** Quantitative results on the NHR [Zhang et al \(2020\)](#) dataset.

Method	NDIN [†] Zhang et al (2014)	GS [†] Li et al (2015)	MRP [†] Zhang et al (2017)	MRP [†] Zhang et al (2017)	OSFD [†] Zhang et al (2020)	HCD Wang et al (2024b)	FocalNet Cui et al (2023a)	Jin et al [†] Jin et al (2023a)	FSNet Cui et al (2023b)	ConvIR-B Cui et al (2024a)	PoolNet-B Cui et al (2025a)	FSNet + UDP (Ours)	ConvIR + UDP (Ours)
PSNR [†]	14.31	17.32	16.95	19.93	21.32	23.43	25.35	26.56	26.30	29.49	28.28	28.09	29.54
SSIM [†]	0.526	0.629	0.667	0.777	0.804	0.953	0.969	0.890	0.976	0.983	0.980	0.980	0.983

[†] Denotes methods that are specially designed for nighttime image dehazing.

Table 6 Quantitative results on real-world datasets: Dense-Haze [Ancuti et al \(2019\)](#) and NH-HAZE [Ancuti et al \(2020\)](#).

Method	Dense-Haze			NH-HAZE		
	PSNR [†]	SSIM [†]	LPIPS [†]	PSNR [†]	SSIM [†]	LPIPS [†]
DehazeNet Cai et al (2016)	13.84	0.43	-	16.62	0.52	-
MSBDN Dong et al (2020)	15.37	0.49	-	19.23	0.71	-
FFA-Net Qin et al (2020)	14.39	0.45	-	19.87	0.69	-
AECR-Net Wu et al (2021)	15.80	0.47	-	19.88	0.72	-
DeHamer Guo et al (2022)	16.62	0.56	0.6346	20.66	0.68	0.3837
PMNet Ye et al (2022)	16.79	0.51	-	20.42	0.73	-
MB-TaylorFormer-B Qiu et al (2023)	16.66	0.56	0.6125	-	-	-
C ² PNet Zheng et al (2023)	16.88	0.57	-	20.24	0.69	-
FocalNet Cui et al (2023a)	17.07	0.63	0.6087	20.43	0.79	0.3780
SFNet Cui et al (2023c)	17.46	0.58	0.5689	20.46	0.80	-
FSNet Cui et al (2023b)	17.13	0.65	0.5756	20.55	0.81	0.3624
ConvIR-S Cui et al (2024a)	17.45	0.65	0.6000	20.65	0.80	0.3669
PGH ² Net Su et al (2025)	17.02	0.61	-	-	-	-
MB-TaylorFormerV2-B Jin et al (2025)	16.95	0.62	-	20.73	0.70	-
ConvIR + UDP (Ours)	17.55	0.67	0.5813	20.98	0.82	0.3567
FSNet + UDP (Ours)	17.85	0.65	0.6033	20.94	0.82	0.3732

state-of-the-art with 43.30 dB PSNR on SOTS-Indoor, while maintaining comparable results on SOTS-Outdoor. These results highlight the effectiveness of our UDP design, achieving a new milestone in image dehazing. Moreover, we further evaluate our approach on the more realistic synthetic Haze4K dataset [Liu et al \(2021a\)](#). Table 3 showcases the performance of our UDP method applied to FSNet. As reported in Table 3, applying our UDP strategy to FSNet yields an average PSNR improvement of 1.19 dB over the original model. In addition, ConvIR + UDP also achieves a competitive PSNR of 34.82 dB. The qualitative comparisons on these daytime datasets, including SOTS-Indoor [Li et al \(2018\)](#), SOTS-Outdoor [Li et al \(2018\)](#), and Haze4K [Liu et al \(2021a\)](#), are illustrated in Figs. 6, 7, and 8, respectively. Our models generate haze-free images that are more visually consistent with the ground truth.

Table 7 Image Dehazing Comparisons on the Remote Sensing Datasets: SateHaze1k-Thin, SateHaze1k-Moderate, and SateHaze1k-Thick [Huang et al \(2020\)](#)

Method	Thin		Moderate		Thick	
	PSNR [†]	SSIM [†]	PSNR [†]	SSIM [†]	PSNR [†]	SSIM [†]
AOD-Net Li et al (2017)	19.54	0.854	20.10	0.885	15.92	0.731
H2RL-Net [†] Chen et al (2021)	20.91	0.880	22.34	0.906	17.41	0.768
FCFT-Net [†] Li and Chen (2020)	23.59	0.913	22.88	0.927	20.03	0.816
Uformer Wang et al (2022)	22.82	0.907	24.47	0.939	20.36	0.815
C ² PNet Zheng et al (2023)	19.62	0.880	24.79	0.940	16.83	0.790
Restormer Zamir et al (2022)	23.08	0.912	24.73	0.933	18.58	0.762
Trinity-Net [†] Chi et al (2023)	21.55	0.884	23.35	0.895	20.97	0.823
UMWTransformer Kulkarni et al (2022)	24.29	0.919	26.65	0.946	20.07	0.825
FocalNet Cui et al (2023a)	24.16	0.916	25.99	0.947	21.69	0.847
ConvIR-S Cui et al (2024a)	25.11	0.978	26.79	0.978	22.65	0.950
PoolNet-S Cui et al (2025a)	25.02	0.979	27.02	0.979	22.73	0.955
ConvIR + UDP (Ours)	25.48	0.979	28.07	0.981	22.95	0.953
PoolNet + UDP (Ours)	26.20	0.980	28.26	0.979	23.13	0.951

[†] Denotes methods that are specially designed for remote sensing image dehazing.

To further demonstrate the superiority of our model, we conduct experiments on two nighttime datasets, *i.e.*, GTA5 [Yan et al \(2020\)](#) and NHR [Zhang et al \(2020\)](#). Table 4 shows that ConvIR + UDP and PoolNet + UDP secure the first and second places with 33.12 dB and 32.78 dB PSNR, surpassing the original counterparts by 1.29 dB and 1.25 dB, respectively. The original models struggle to achieve optimal results under low-light conditions. However, by incorporating our UDP



Figure 10 Nighttime image dehazing comparisons on the NHR [Zhang et al \(2020\)](#) dataset.

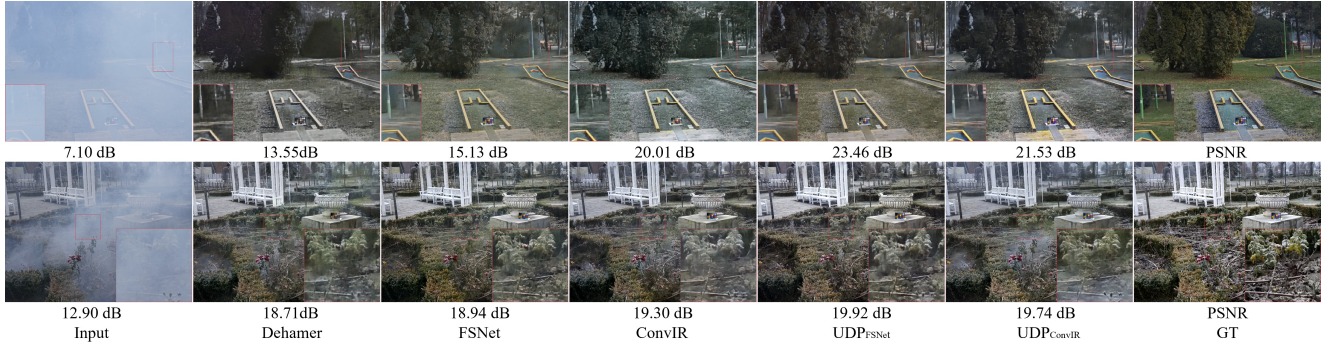


Figure 11 Qualitative comparisons on the Dense-Haze [Ancuti et al \(2019\)](#) dataset and NH-HAZE [Ancuti et al \(2020\)](#) dataset among DeHamer [Guo et al \(2022\)](#), FSNet [Cui et al \(2023b\)](#), ConvIR [Cui et al \(2024a\)](#), and ours.

approach, we effectively alleviate these limitations, enhancing the overall brightness and recovering fine image details. The visual comparisons in Fig. 9 further confirm the effectiveness of our design, as the images generated by our models are much closer to the ground truth. We further extensively compare our models with state-of-the-art methods on real-world datasets. As shown in Table 6, our methods achieve state-of-the-art performance on both Dense-Haze [Ancuti et al \(2019\)](#) and NH-HAZE [Ancuti et al \(2020\)](#). On Dense-Haze, FSNet + UDP obtains 17.85 dB PSNR, surpassing FSNet by 0.72 dB. On NH-HAZE, ConvIR + UDP achieves the best performance with 20.98 dB PSNR, outperforming the previous best MB-TaylorFormerV2-B [Jin et al \(2025\)](#), and also attains the best perceptual quality. These results clearly demonstrate the effectiveness of our UDP in boosting real-world dehazing performance. The visual comparisons are shown in Fig. 11.

Since image dehazing is crucial for remote sensing applications, we further evaluate our models on the SateHaze1k [Huang et al \(2020\)](#) dataset in Table 7. Our methods consistently achieve the best results across all three subsets. In particular, PoolNet + UDP attains 26.20 dB, 28.26 dB, and 23.13 dB PSNR on the three subsets, outperforming both general dehazing models (*e.g.*, FocalNet [Cui et al \(2023a\)](#), ConvIR-S [Cui et al \(2024b\)](#)) and remote sensing-oriented designs (*e.g.*,

Trinity-Net [Chi et al \(2023\)](#)). Notably, on the challenging Thick subset, our method achieves a gain of 1.44 dB over FocalNet, highlighting its strong generalization capability to remote sensing scenarios.

To further demonstrate the robustness and superiority of our approach, we conduct experiments on the all-in-one setting [Jiang et al \(2025\)](#). This fundamental setting evaluates the ability of a single model to function as a universal and versatile restorer. In our study, we adopt the more challenging five-task benchmark, which jointly considers Gaussian denoising, deraining, dehazing, motion deblurring, and low-light enhancement, thus requiring stronger generalization from a single set of model weights. As shown in Table 8, both PromptIR + UDP and AdaIR + UDP achieve substantial improvements in dehazing and low-light enhancement, with PromptIR + UDP yields further gains in deraining and AdaIR + UDP further boosting performance in motion deblurring. This can be largely attributed to the integration of depth-based priors, which promote a more nuanced understanding of global atmospheric illumination and fine-grained object structures. Although originally introduced to enhance dehazing, such priors also strengthen the model’s ability to recover structural fidelity in motion deblurring and illumination details in low-light enhancement. Consequently, AdaIR + UDP surpasses its original

Table 8 Performance comparison of different methods on five challenging benchmarks. Denoising results are reported at $\sigma = 25$. The baseline results are in blue. Best results are **highlighted**.

Method	Dehazing on SOTS		Deraining on Rain100L		Denoising on BSD68		Deblurring on GoPro		Low-Light on LOL		Average	
	Li et al (2018) PSNR	SSIM	Yang et al (2019) PSNR	SSIM	Martin et al (2001) PSNR	SSIM	Nah et al (2017) PSNR	SSIM	Wei et al (2018) PSNR	SSIM	PSNR	SSIM
(TIP'23) DehazeFormer Song et al (2023)	25.31	0.937	33.68	0.954	30.89	0.880	25.93	0.785	21.31	0.819	27.42	0.875
(ICCV'23) Retinexformer Cai et al (2023)	24.81	0.933	32.68	0.940	30.84	0.880	25.09	0.779	22.76	0.863	27.24	0.873
(ICCVW'21) SwinIR Liang et al (2021)	21.50	0.891	30.78	0.923	30.59	0.868	24.52	0.773	17.81	0.723	25.04	0.835
(CVPR'22) DGUNet Mou et al (2022)	24.78	0.940	36.62	0.971	31.10	0.883	27.25	0.837	21.87	0.823	28.32	0.891
(CVPR'22) Restormer Zamir et al (2022)	24.09	0.927	34.81	0.960	31.49	0.884	27.22	0.829	20.41	0.806	27.60	0.881
(ECCV'22) NAFNet Chen et al (2022)	25.23	0.939	35.56	0.967	31.02	0.883	26.53	0.808	20.49	0.809	27.76	0.881
(TPAMI'23) FSNet Cui et al (2023b)	25.53	0.943	36.07	0.968	31.33	0.883	28.32	0.869	22.29	0.829	28.71	0.898
(TPAMI'19) DL Fan et al (2019)	20.54	0.826	21.96	0.762	23.09	0.745	19.86	0.672	19.83	0.712	21.05	0.743
(CVPR'22) Transweather Valanarasu et al (2022)	21.32	0.885	29.43	0.905	29.00	0.841	25.12	0.757	21.21	0.792	25.22	0.836
(CVPR'22) AirNet Li et al (2022)	21.04	0.884	32.98	0.951	30.91	0.882	24.35	0.781	18.18	0.735	25.49	0.846
(NeurIPS'23) PromptIR Potlapalli et al (2023)	26.54	0.949	36.37	0.970	31.47	0.886	28.71	0.881	22.68	0.832	29.15	0.904
(ICLR'25) AdaIR Cui et al (2025b)	30.53	0.978	38.02	0.981	31.35	0.889	28.12	0.858	23.00	0.845	30.20	0.910
(ICLR'25) DCPT_PromptIR Hu et al (2025)	30.72	0.977	37.32	0.978	31.32	0.885	28.84	0.877	23.35	0.840	30.31	0.911
(TPAMI'25) DA-RCOT Tang et al (2025)	30.96	0.975	37.87	0.980	31.23	0.888	28.68	0.872	23.25	0.836	30.40	0.911
(TIP'25) Perceive-IR Zhang et al (2025)	28.19	0.964	37.25	0.977	31.44	0.887	29.46	0.886	22.88	0.833	29.84	0.909
(TIP'25) Pool-AIO Cui et al (2025a)	30.25	0.977	37.85	0.981	31.24	0.887	27.66	0.844	22.66	0.841	29.93	0.906
(TIP'25) DPPD_PromptIR Wu et al (2025)	30.31	0.980	37.32	0.980	31.33	0.885	28.74	0.875	22.73	0.846	30.09	0.913
(CVPR'25) VLU-Net Zeng et al (2025)	30.84	0.980	38.54	0.982	31.43	0.891	27.46	0.840	22.29	0.833	30.11	0.905
(Ours) PromptIR + UDP	31.33	0.980	37.63	0.980	31.25	0.883	28.34	0.868	23.18	0.851	30.35	0.912
(Ours) AdaIR + UDP	31.41	0.980	37.85	0.980	31.28	0.888	28.62	0.870	23.53	0.854	30.55	0.915

Table 9 Ablation analysis on different variants of our method, mainly including two aspects: fusion stages and attention types. Here, all ablation models adopt the backbone of FSNet Cui et al (2023b).

Head	Encoder					Decoder				Backbone	Metrics		
	concat	DGAM	CCA _{depth}	CCA _{rgb}	SCA _{depth}	SCA _{rgb}	CCA _{depth}	CCA _{rgb}	SCA _{depth}	SCA _{rgb}	PSNR	SSIM	
(a)	✗	✗	✗	✗	✗	✗	✗	✗	✗	✗	✓	34.12	0.9901
(b)	✓	✗	✗	✗	✗	✗	✗	✗	✗	✗	✓	34.78	0.9908
(c)	✗	✓	✗	✗	✗	✗	✗	✗	✗	✗	✓	34.96	0.9908
(d)	✗	✓	✓	✓	✗	✗	✗	✗	✗	✗	✓	34.93	0.9908
(e)	✗	✓	✗	✓	✗	✗	✗	✗	✗	✗	✓	35.06	0.9910
(f)	✗	✓	✗	✗	✓	✗	✗	✗	✗	✗	✓	35.10	0.9907
(g)	✗	✓	✗	✗	✗	✓	✗	✗	✗	✗	✓	35.13	0.9910
(h)	✗	✓	✗	✗	✗	✗	✓	✗	✗	✗	✓	34.94	0.9909
(i)	✗	✓	✗	✗	✗	✗	✗	✓	✗	✗	✓	34.99	0.9907
(j)	✗	✓	✗	✗	✗	✗	✗	✗	✓	✗	✓	34.92	0.9909
(k)	✗	✓	✗	✗	✗	✗	✗	✗	✗	✓	✓	35.02	0.9910
(l)	✗	✓	✗	✗	✓	✓	✗	✗	✗	✗	✓	35.22	0.9908

counterpart and establishes a new benchmark for all-in-one image restoration.

5.4 Ablation Study

We conduct ablation studies to demonstrate the effectiveness of the proposed UDPNet by training and testing the models on the Haze4K dataset Liu et al (2021a). The model is trained for 1000 epochs using FSNet Cui et al (2023b) as the baseline.

5.4.1 Contribution of the Depth Map

The first step in our analysis is to justify the integration of depth information. As shown in Table 10, the baseline model FSNet achieves a PSNR of 34.12 dB. By incorporating depth maps extracted using the DepthAnything-V2-small variant together with our proposed UDP, the model's performance is improved to 34.69 dB, while only introducing 0.32 M parameters. Although the gain at this stage is relatively modest, it demonstrates the effectiveness of depth priors. Using the base and large variants of DepthAnything V2 further increases performance, reaching 34.87 dB and a peak of

Table 10 Comparison of different depth maps. All depth variants have an identical parameter increase of only +0.32M.

Methods	Baseline (13.28M)	Grey (13.60M)	Small (13.60M)	Base (13.60M)	Large (13.60M)
PSNR	34.12 dB	34.08 dB	34.69 dB	34.87 dB	35.31 dB

35.31 dB, respectively. In contrast, when the depth map is replaced with a 128-level gray map, the performance drops to 34.08 dB, highlighting that the performance improvement comes from accurate depth information rather than the increase in parameter count. Overall, these results confirm that accurate depth estimation is a key factor in image dehazing.

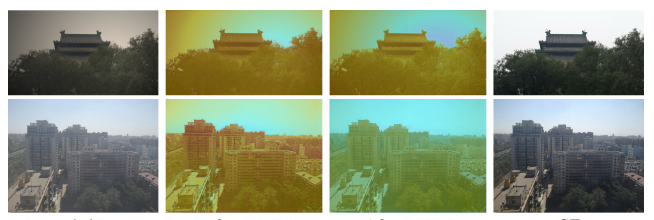


Figure 12 Illustrations of intermediate features. The proposed DPFM effectively generates features with enhanced textures, sharper edges, and clearer global structures, thereby facilitating high-quality reconstruction.

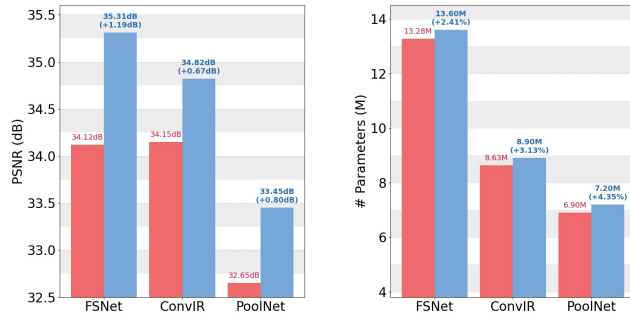


Figure 13 Performance and efficiency variations with our UDP on the Haze4K dataset, compared with baseline methods [Cui et al \(2023b, 2024a, 2025a\)](#).

5.4.2 Effectiveness of each module

We perform the breakdown ablations by applying our modules to the baseline successively. The number of heads in the multi-head attention is set to 1, while all other configurations remain identical to the final dehazing model. As shown in Table 9, directly concatenating refined depth maps and RGB images at the network head (row (b)) significantly improves performance compared to the baseline (row (a)), reaching 34.78 dB PSNR. This demonstrates the substantial benefit of introducing depth maps for image dehazing. By contrast, replacing simple concatenation with the proposed DGAM (row (c)) yields further gains with 34.96 dB PSNR, verifying that adaptively weighting depth cues through channel attention is more effective than naive feature stacking.

We further explore two variants of DPFM: channel cross-attention (CCA) and spatial cross-attention (SCA). Results in rows (d–g) show that both variants outperform DGAM, indicating the benefit of explicitly modeling cross-modal dependencies. Notably, using RGB features as the query (CCA_{rgb} , SCA_{rgb}) consistently outperforms the depth-as-query counterparts, suggesting that RGB semantics provide a more reliable guidance signal. Moreover, spatial cross-attention (SCA) shows slightly higher gains than channel cross-attention (CCA), suggesting that spatial correspondences play a crucial role in depth–RGB fusion. Across all cases, the best performance 35.22 dB PSNR is achieved in row (l), where both SCA_{depth} and SCA_{rgb} are combined in the encoder, highlighting the complementarity of depth and RGB at the spatial level and confirming the necessity of deliberate design for depth map integration.

Finally, we provide a visualization of the intermediate features to further demonstrate the effectiveness of the proposed DPFM, as shown in Figure 12. Specifically, the features are extracted from the first encoder before and after applying our DPFM. Moreover, Figure 13 illustrates that our UDP, as a plugin, can be seamlessly

integrated into off-the-shelf methods to improve their performance while avoiding a significant increase in the number of parameters.

5.4.3 Position of DPFM

We also investigate inserting DPFM into different network stages. Placing DPFM in the encoder (rows (d–g)) yields more notable gains in Table 9, since incorporating depth priors at early stages enhances semantic abstraction and provides stronger guidance for subsequent layers. By contrast, applying DPFM to the decoder (rows (h–k)) still brings consistent improvements, but the benefits are relatively smaller. This can be attributed to the fact that depth maps mainly contain low-frequency structural cues, which may interfere with the reconstruction of high-frequency image details when introduced in the decoder.

5.4.4 Impact of the number of heads in DPFM

We investigate the effect of varying the number of attention heads in the multi-head overlapping cross-attention of DPFM. Specifically, we evaluate configurations with 1, 2, and 4 heads. When using a single head, the model achieves 35.20 dB PSNR. Increasing the number of heads to 2 yields the best performance of 35.31 dB PSNR, suggesting that multiple attention heads can capture complementary correlations between RGB and depth features more effectively. Further increasing to 4 heads slightly decreases the PSNR to 35.27 dB. Overall, these results demonstrate that a moderate number of attention heads is sufficient to fully exploit cross-modal dependencies while maintaining high-frequency detail reconstruction.

5.4.5 Generalization of our proposed UDP

To evaluate the adaptability of the proposed UDP, we integrate it into different baseline models, including FSNet [Cui et al \(2023b\)](#), ConvIR [Cui et al \(2024a\)](#), PoolNet [Cui et al \(2025a\)](#), PromptIR [Potlapalli et al \(2023\)](#) and AdaIR [Cui et al \(2025b\)](#). Each modified network is then trained and tested under the same experimental settings. The comparative results demonstrate that UDP can not only be applied to a variety of multi-scale image restoration networks but also effectively enhance the performance of all-in-one image restoration models, yielding improvements in tasks such as dehazing, deblurring, deraining, and low-light enhancement.

5.5 Limitations

Our work introduces a novel method for image dehazing by effectively leveraging depth-based priors, which significantly enhance model adaptability and performance through plug-and-play modules. By integrating depth features, our approach lays the foundation for developing more robust and versatile dehazing models. However, the UDP framework has several limitations that open avenues for future research. One key limitation is the reliance on depth priors extracted from degraded images, which may introduce inaccuracies due to noise or occlusions in the depth estimation process. These inaccuracies could lead to structural distortions or loss of fine details in the restored image. Furthermore, the dependence on DepthAnything V2 priors during inference introduces computational inefficiency, as the external model requires additional resources for depth estimation, increasing inference time. Future work could explore alternative strategies for real-time depth inference or distilling depth priors from depth estimation models into image restoration models. While the UDP framework demonstrates promising results across various restoration tasks, the potential of leveraging depth-based priors for general image restoration remains an exciting direction. Future studies will focus on refining adaptive strategies to improve performance in a broader range of image restoration scenarios, with particular attention to enhancing real-time performance and reducing reliance on external depth models.

6 Conclusion

In recent years, the field of single-image dehazing has witnessed significant advancements, primarily driven by effective module design. However, the utilization of multimodal information remains limited, and depth information that is closely tied to the physical process of haze formation is often overlooked. In this paper, we present UDPNet, a general framework guided by depth priors for image dehazing to enhance multi-scale, multi-shape, and dual-modal representation learning. Our approach integrates a large-scale pre-trained depth estimation model to extract scene depth priors, which are utilized within diverse U-shaped network architectures. By leveraging efficient fusion strategies, we adaptively tailor the model to handle different haze distributions. These combined innovations yield a robust solution for image dehazing, as demonstrated by our extensive evaluations, while also showcasing the potential of our framework for universal image restoration. Our future work will explore the framework in other image restoration tasks.

References

Ancuti C, Ancuti CO, De Vleeschouwer C, Bovik AC (2016) Night-time dehazing by fusion. In: 2016 IEEE international conference on image processing (ICIP), IEEE, pp 2256–2260

Ancuti CO, Ancuti C, Sbert M, Timofte R (2019) Dense-Haze: A benchmark for image dehazing with dense-haze and haze-free images. In: 2019 IEEE international conference on image processing (ICIP), IEEE, pp 1014–1018

Ancuti CO, Ancuti C, Timofte R (2020) NH-HAZE: An image dehazing benchmark with non-homogeneous hazy and haze-free images. In: Proceedings of the IEEE/CVF conference on computer vision and pattern recognition workshops, pp 444–445

Berman D, Treibitz T, Avidan S (2018) Single image dehazing using haze-lines. *IEEE transactions on pattern analysis and machine intelligence* 42(3):720–734

Bhat SF, Alhashim I, Wonka P (2021) AdaBins: Depth estimation using adaptive bins. In: Proceedings of the IEEE/CVF conference on computer vision and pattern recognition, pp 4009–4018

Birk R, Wofk D, Müller M (2023) MiDaS v3.1 – a model zoo for robust monocular relative depth estimation. *arXiv preprint arXiv:230714460*

Cai B, Xu X, Jia K, Qing C, Tao D (2016) DehazeNet: An end-to-end system for single image haze removal. *IEEE transactions on image processing* 25(11):5187–5198

Cai Y, Bian H, Lin J, Wang H, Timofte R, Zhang Y (2023) Retinexformer: One-stage retinex-based transformer for low-light image enhancement. In: Proceedings of the IEEE/CVF international conference on computer vision, pp 12504–12513

Chen L, Chu X, Zhang X, Sun J (2022) Simple baselines for image restoration. In: European conference on computer vision, Springer, pp 17–33

Chen X, Li Y, Dai L, Kong C (2021) Hybrid high-resolution learning for single remote sensing satellite image dehazing. *IEEE geoscience and remote sensing letters* 19:1–5

Chen X, Wang X, Zhou J, Qiao Y, Dong C (2023) Activating more pixels in image super-resolution transformer. In: Proceedings of the IEEE/CVF conference on computer vision and pattern recognition, pp 22367–22377

Chen Z, He Z, Lu ZM (2024) DEA-Net: Single image dehazing based on detail-enhanced convolution and content-guided attention. *IEEE transactions on image processing* 33:1002–1015

Cheng L, Zhao L (2021) Two-stage image dehazing with depth information and cross-scale non-local attention. In: 2021 IEEE International Conference on Big Data (Big Data), IEEE, pp 3155–3162

Chi K, Yuan Y, Wang Q (2023) Trinity-Net: Gradient-guided swin transformer-based remote sensing image dehazing and beyond. *IEEE Transactions on Geoscience and Remote Sensing* 61:1–14

Cui Y, Ren W, Cao X, Knoll A (2023a) Focal network for image restoration. In: Proceedings of the IEEE/CVF international conference on computer vision, pp 13001–13011

Cui Y, Ren W, Cao X, Knoll A (2023b) Image restoration via frequency selection. *IEEE Transactions on Pattern Analysis and Machine Intelligence* 46(2):1093–1108

Cui Y, Tao Y, Bing Z, Ren W, Gao X, Cao X, Huang K, Knoll A (2023c) Selective frequency network for image restoration. In: The eleventh international conference on learning representations

Cui Y, Ren W, Cao X, Knoll A (2024a) Revitalizing convolutional network for image restoration. *IEEE Transactions on Pattern Analysis and Machine Intelligence*

Cui Y, Ren W, Knoll A (2024b) Omni-kernel network for image restoration. In: Proceedings of the AAAI Conference on Artificial Intelligence, vol 38, pp 1426–1434

Cui Y, Ren W, Knoll A (2025a) Exploring the potential of pooling techniques for universal image restoration. *IEEE Transactions on Image Processing*

Cui Y, Zamir SW, Khan S, Knoll A, Shah M, Khan FS (2025b) AdaIR: Adaptive all-in-one image restoration via frequency mining and modulation. In: The Thirteenth International Conference on Learning Representations

Dong H, Pan J, Xiang L, Hu Z, Zhang X, Wang F, Yang MH (2020) Multi-scale boosted dehazing network with dense feature fusion. In: Proceedings of the IEEE/CVF conference on computer vision and pattern recognition, pp 2157–2167

Du R, Wang H, Liu W, Wang G, Jiang K, Ko H (2025) Image dehazing via rgb-fir multimodal fusion and collaborative learning. *Pattern Recognition* p 112206

Dudhane A, Murala S (2019) RYF-Net: Deep fusion network for single image haze removal. *IEEE Transactions on Image Processing* 29:628–640

Fan Q, Chen D, Yuan L, Hua G, Yu N, Chen B (2019) A general decoupled learning framework for parameterized image operators. *IEEE transactions on pattern analysis and machine intelligence* 43(1):33–47

Fang W, Fan J, Zheng Y, Weng J, Tai Y, Li J (2025) Guided real image dehazing using ycbcr color space. In: Proceedings of the AAAI Conference on Artificial Intelligence, vol 39, pp 2906–2914

Feng C, Zhuo S, Zhang X, Shen L, Süsstrunk S (2013) Near-infrared guided color image dehazing. In: 2013 IEEE international conference on image processing, IEEE, pp 2363–2367

Geiger A, Lenz P, Stiller C, Urtasun R (2013) Vision meets robotics: The KITTI dataset. *The international journal of robotics research* 32(11):1231–1237

Guo CL, Yan Q, Anwar S, Cong R, Ren W, Li C (2022) Image dehazing transformer with transmission-aware 3d position embedding. In: Proceedings of the IEEE/CVF conference on computer vision and pattern recognition, pp 5812–5820

He K, Sun J, Tang X (2010) Single image haze removal using dark channel prior. *IEEE transactions on pattern analysis and machine intelligence* 33(12):2341–2353

He K, Sun J, Tang X (2012) Guided image filtering. *IEEE transactions on pattern analysis and machine intelligence* 35(6):1397–1409

Hong M, Xie Y, Li C, Qu Y (2020) Distilling image dehazing with heterogeneous task imitation. In: Proceedings of the IEEE/CVF conference on computer vision and pattern recognition, pp 3462–3471

Hu J, Jin L, Yao Z, Lu Y (2025) Universal image restoration pre-training via degradation classification. *arXiv preprint arXiv:250115510*

Huang B, Zhi L, Yang C, Sun F, Song Y (2020) Single satellite optical imagery dehazing using sar image prior based on conditional generative adversarial networks. In: Proceedings of the IEEE/CVF winter conference on applications of computer vision, pp 1806–1813

Jiang J, Zuo Z, Wu G, Jiang K, Liu X (2025) A survey on all-in-one image restoration: Taxonomy, evaluation and future trends. *IEEE Transactions on Pattern Analysis and Machine Intelligence*

Jin Y, Lin B, Yan W, Yuan Y, Ye W, Tan RT (2023a) Enhancing visibility in nighttime haze images using guided apsf and gradient adaptive convolution. In: Proceedings of the 31st ACM international conference on multimedia, pp 2446–2457

Jin Z, Chen S, Chen Y, Xu Z, Feng H (2023b) Let segment anything help image dehaze. *arXiv preprint arXiv:230615870*

Jin Z, Qiu Y, Zhang K, Li H, Luo W (2025) MB-TaylorFormer V2: Improved multi-branch linear transformer expanded by taylor formula for image restoration. *arXiv preprint arXiv:250104486*

Ju M, Ding C, Guo YJ, Zhang D (2019) IDGCP: Image dehazing based on gamma correction prior. *IEEE*

Transactions on Image Processing 29:3104–3118

Krizhevsky A, Sutskever I, Hinton GE (2012) Imagenet classification with deep convolutional neural networks. *Advances in neural information processing systems* 25

Kulkarni A, Phutke SS, Murala S (2022) Unified transformer network for multi-weather image restoration. In: *European Conference on Computer Vision*, Springer, pp 344–360

Lee BU, Lee K, Oh J, Kweon IS (2020) Cnn-based simultaneous dehazing and depth estimation. In: *2020 IEEE international conference on robotics and automation (ICRA)*, IEEE, pp 9722–9728

Li B, Peng X, Wang Z, Xu J, Feng D (2017) AOD-Net: All-in-one dehazing network. In: *Proceedings of the IEEE international conference on computer vision*, pp 4770–4778

Li B, Ren W, Fu D, Tao D, Feng D, Zeng W, Wang Z (2018) Benchmarking single-image dehazing and beyond. *IEEE Transactions on Image Processing* 28(1):492–505

Li B, Gou Y, Gu S, Liu JZ, Zhou JT, Peng X (2021) You only look yourself: Unsupervised and untrained single image dehazing neural network. *International Journal of Computer Vision* 129(5):1754–1767

Li B, Liu X, Hu P, Wu Z, Lv J, Peng X (2022) All-in-one image restoration for unknown corruption. In: *Proceedings of the IEEE/CVF conference on computer vision and pattern recognition*, pp 17452–17462

Li P, Tian J, Tang Y, Wang G, Wu C (2020) Deep retinex network for single image dehazing. *IEEE Transactions on Image Processing* 30:1100–1115

Li Y, Chen X (2020) A coarse-to-fine two-stage attentive network for haze removal of remote sensing images. *IEEE Geoscience and Remote Sensing Letters* 18(10):1751–1755

Li Y, Tan RT, Brown MS (2015) Nighttime haze removal with glow and multiple light colors. In: *Proceedings of the IEEE international conference on computer vision*, pp 226–234

Li Y, Wang X, Wang J, Chang Y, Cao K, Yan L (2025) Hierarchical semantic-visual fusion of visible and near-infrared images for long-range haze removal. *arXiv preprint arXiv:250703893*

Liang J, Cao J, Sun G, Zhang K, Van Gool L, Timofte R (2021) SwinIR: Image restoration using swin transformer. In: *Proceedings of the IEEE/CVF international conference on computer vision*, pp 1833–1844

Lin B, Jin Y, Wending Y, Ye W, Yuan Y, Tan RT (2025) NightHaze: Nighttime image dehazing via self-prior learning. In: *Proceedings of the AAAI Conference on Artificial Intelligence*, vol 39, pp 5209–5217

Liu H, Hu HM, Jiang Y, Liu Y (2025) PEIE: Physics embedded illumination estimation for adaptive dehazing. In: *Proceedings of the AAAI Conference on Artificial Intelligence*, vol 39, pp 5469–5477

Liu J, Wu H, Xie Y, Qu Y, Ma L (2020) Trident dehazing network. In: *Proceedings of the IEEE/CVF Conference on Computer Vision and Pattern Recognition Workshops*, pp 430–431

Liu X, Ma Y, Shi Z, Chen J (2019) GridDehazeNet: Attention-based multi-scale network for image dehazing. In: *Proceedings of the IEEE/CVF international conference on computer vision*, pp 7314–7323

Liu Y, Zhu L, Pei S, Fu H, Qin J, Zhang Q, Wan L, Feng W (2021a) From synthetic to real: Image dehazing collaborating with unlabeled real data. In: *Proceedings of the 29th ACM international conference on multimedia*, pp 50–58

Liu Y, Yan Z, Chen S, Ye T, Ren W, Chen E (2023) NightHazeFormer: Single nighttime haze removal using prior query transformer. In: *Proceedings of the 31st ACM International Conference on Multimedia*, pp 4119–4128

Liu Z, Lin Y, Cao Y, Hu H, Wei Y, Zhang Z, Lin S, Guo B (2021b) Swin Transformer: Hierarchical vision transformer using shifted windows. In: *Proceedings of the IEEE/CVF international conference on computer vision*, pp 10012–10022

Loshchilov I, Hutter F (2016) SGDR: Stochastic gradient descent with warm restarts. *arXiv preprint arXiv:160803983*

Luo P, Xiao G, Gao X, Wu S (2023) LKD-Net: Large kernel convolution network for single image dehazing. In: *2023 IEEE International Conference on Multimedia and Expo (ICME)*, IEEE, pp 1601–1606

Ma K, Duanmu Z, Wu Q, Wang Z, Yong H, Li H, Zhang L (2016) Waterloo exploration database: New challenges for image quality assessment models. *IEEE Transactions on Image Processing* 26(2):1004–1016

Martin D, Fowlkes C, Tal D, Malik J (2001) A database of human segmented natural images and its application to evaluating segmentation algorithms and measuring ecological statistics. In: *Proceedings eighth IEEE international conference on computer vision. ICCV 2001*, IEEE, vol 2, pp 416–423

Meng G, Wang Y, Duan J, Xiang S, Pan C (2013) Efficient image dehazing with boundary constraint and contextual regularization. In: *Proceedings of the IEEE international conference on computer vision*, pp 617–624

Middleton WEK (1957) Vision through the atmosphere. In: *geophysik ii/geophysics ii*, Springer, pp 254–287

Mo Y, Li C, Zheng Y, Wu X (2022) DCA-CycleGAN: Unsupervised single image dehazing using dark channel attention optimized cyclegan. *Journal of Visual Communication and Image Representation* 82:103431

Mou C, Wang Q, Zhang J (2022) Deep generalized unfolding networks for image restoration. In: *Proceedings of the IEEE/CVF conference on computer vision and pattern recognition*, pp 17399–17410

Nah S, Hyun Kim T, Mu Lee K (2017) Deep multi-scale convolutional neural network for dynamic scene deblurring. In: *Proceedings of the IEEE conference on computer vision and pattern recognition*, pp 3883–3891

Quab M, Darcet T, Moutakanni T, Vo H, Szafraniec M, Khalidov V, Fernandez P, Haziza D, Massa F, El-Nouby A, et al (2023) DINOv2: Learning robust visual features without supervision. *arXiv preprint arXiv:230407193*

Pang Y, Xie J, Li X (2018) Visual haze removal by a unified generative adversarial network. *IEEE Transactions on Circuits and Systems for Video Technology* 29(11):3211–3221

Paszke A (2019) Pytorch: An imperative style, high-performance deep learning library. *arXiv preprint arXiv:191201703*

Potlapalli V, Zamir SW, Khan S, Khan F (2023) PromptIR: Prompting for all-in-one image restoration. In: *Thirty-seventh Conference on Neural Information Processing Systems*

Qin X, Wang Z, Bai Y, Xie X, Jia H (2020) FFA-Net: Feature fusion attention network for single image dehazing. In: *Proceedings of the AAAI conference on artificial intelligence*, vol 34, pp 11908–11915

Qiu Y, Zhang K, Wang C, Luo W, Li H, Jin Z (2023) Mb-TaylorFormer: Multi-branch efficient transformer expanded by taylor formula for image dehazing. In: *Proceedings of the IEEE/CVF International Conference on Computer Vision*, pp 12802–12813

Qu Y, Chen Y, Huang J, Xie Y (2019) Enhanced pix2pix dehazing network. In: *Proceedings of the IEEE/CVF conference on computer vision and pattern recognition*, pp 8160–8168

Ren W, Liu S, Zhang H, Pan J, Cao X, Yang MH (2016) Single image dehazing via multi-scale convolutional neural networks. In: *Computer Vision–ECCV 2016: 14th European Conference, Amsterdam, The Netherlands, October 11–14, 2016, Proceedings, Part II* 14, Springer, pp 154–169

Ren W, Pan J, Zhang H, Cao X, Yang MH (2020) Single image dehazing via multi-scale convolutional neural networks with holistic edges. *International Journal of Computer Vision* 128(1):240–259

Shen H, Ding H, Zhang Y, Zhao ZQ, Jiang X (2025) Spatial frequency modulation network for efficient image dehazing. *IEEE Transactions on Image Processing*

Silberman N, Hoiem D, Kohli P, Fergus R (2012) Indoor segmentation and support inference from rgbd images. In: *Computer Vision–ECCV 2012: 12th European Conference on Computer Vision, Florence, Italy, October 7–13, 2012, Proceedings, Part V* 12, Springer, pp 746–760

Song Y, He Z, Qian H, Du X (2023) Vision transformers for single image dehazing. *IEEE Transactions on Image Processing* 32:1927–1941

Su X, Li S, Cui Y, Cao M, Zhang Y, Chen Z, Wu Z, Wang Z, Zhang Y, Yuan X (2025) Prior-guided hierarchical harmonization network for efficient image dehazing. In: *Proceedings of the AAAI Conference on Artificial Intelligence*, vol 39, pp 7042–7050

Tang X, Gu X, He X, Hu X, Sun J (2025) Degradation-aware residual-conditioned optimal transport for unified image restoration. *IEEE Transactions on Pattern Analysis and Machine Intelligence*

Tsai FJ, Peng YT, Lin YY, Lin CW (2025) PHATNet: A physics-guided haze transfer network for domain-adaptive real-world image dehazing. In: *Proceedings of the IEEE/CVF international conference on computer vision*

Tu Z, Talebi H, Zhang H, Yang F, Milanfar P, Bovik A, Li Y (2022) MAXIM: Multi-axis mlp for image processing. In: *Proceedings of the IEEE/CVF conference on computer vision and pattern recognition*, pp 5769–5780

Valanarasu JMJ, Yasarla R, Patel VM (2022) TransWeather: Transformer-based restoration of images degraded by adverse weather conditions. In: *Proceedings of the IEEE/CVF conference on computer vision and pattern recognition*, pp 2353–2363

Vaswani A, Shazeer N, Parmar N, Uszkoreit J, Jones L, Gomez AN, Kaiser L, Polosukhin I (2017) Attention is all you need. *Advances in neural information processing systems* 30

Wang C, Pan J, Lin W, Dong J, Wang W, Wu XM (2024a) SelfPromer: Self-prompt dehazing transformers with depth-consistency. In: *Proceedings of the AAAI Conference on Artificial Intelligence*, vol 38, pp 5327–5335

Wang J, Li C, Xu S (2021) An ensemble multi-scale residual attention network (emra-net) for image dehazing. *Multimedia Tools and Applications* 80(19):29299–29319

Wang R, Zheng Y, Zhang Z, Li C, Liu S, Zhai G, Liu X (2025a) Learning hazing to dehazing: Towards realistic

haze generation for real-world image dehazing. In: Proceedings of the Computer Vision and Pattern Recognition Conference, pp 23091–23100

Wang T, Tao G, Lu W, Zhang K, Luo W, Zhang X, Lu T (2024b) Restoring vision in hazy weather with hierarchical contrastive learning. *Pattern Recognition* 145:109956

Wang T, Zhang K, Shao Z, Luo W, Stenger B, Lu T, Kim TK, Liu W, Li H (2024c) GridFormer: Residual dense transformer with grid structure for image restoration in adverse weather conditions. *International journal of computer vision* 132(10):4541–4563

Wang X, Yang G, Ye T, Liu Y (2025b) Dehaze-RetinexGAN: Real-world image dehazing via retinex-based generative adversarial network. In: Proceedings of the AAAI Conference on Artificial Intelligence, vol 39, pp 7997–8005

Wang Z, Bovik AC, Sheikh HR, Simoncelli EP (2004) Image quality assessment: from error visibility to structural similarity. *IEEE transactions on image processing* 13(4):600–612

Wang Z, Cun X, Bao J, Zhou W, Liu J, Li H (2022) Uformer: A general u-shaped transformer for image restoration. In: Proceedings of the IEEE/CVF conference on computer vision and pattern recognition, pp 17683–17693

Wei C, Wang W, Yang W, Liu J (2018) Deep retinex decomposition for low-light enhancement. *arXiv preprint arXiv:180804560*

Wu G, Jiang J, Jiang K, Liu X, Nie L (2025) Learning dynamic prompts for all-in-one image restoration. *IEEE Transactions on Image Processing*

Wu H, Qu Y, Lin S, Zhou J, Qiao R, Zhang Z, Xie Y, Ma L (2021) Contrastive learning for compact single image dehazing. In: Proceedings of the IEEE/CVF conference on computer vision and pattern recognition, pp 10551–10560

Wu RQ, Duan ZP, Guo CL, Chai Z, Li C (2023) RIDCP: Revitalizing real image dehazing via high-quality codebook priors. In: Proceedings of the IEEE/CVF conference on computer vision and pattern recognition, pp 22282–22291

Yan W, Tan RT, Dai D (2020) Nighttime defogging using high-low frequency decomposition and grayscale-color networks. In: European Conference on Computer Vision, Springer, pp 473–488

Yang F, Zhang Q (2022) Depth aware image dehazing. *The Visual Computer* 38(5):1579–1587

Yang L, Kang B, Huang Z, Xu X, Feng J, Zhao H (2024a) Depth Anything: Unleashing the power of large-scale unlabeled data. In: CVPR

Yang L, Kang B, Huang Z, Zhao Z, Xu X, Feng J, Zhao H (2024b) Depth Anything V2. *arXiv:240609414*

Yang W, Tan RT, Feng J, Guo Z, Yan S, Liu J (2019) Joint rain detection and removal from a single image with contextualized deep networks. *IEEE transactions on pattern analysis and machine intelligence* 42(6):1377–1393

Yang Y, Wang C, Liu R, Zhang L, Guo X, Tao D (2022) Self-augmented unpaired image dehazing via density and depth decomposition. In: Proceedings of the IEEE/CVF conference on computer vision and pattern recognition, pp 2037–2046

Yang Y, Wang C, Guo X, Tao D (2024c) Robust unpaired image dehazing via density and depth decomposition. *International Journal of Computer Vision* 132(5):1557–1577

Ye T, Zhang Y, Jiang M, Chen L, Liu Y, Chen S, Chen E (2022) Perceiving and modeling density for image dehazing. In: European conference on computer vision, Springer, pp 130–145

Ye T, Chen S, Chen H, Chai W, Ren J, Xing Z, Li W, Zhu L (2025) PromptHaze: Prompting real-world dehazing via depth anything model. In: Proceedings of the AAAI Conference on Artificial Intelligence, vol 39, pp 9454–9462

Zamir SW, Arora A, Khan S, Hayat M, Khan FS, Yang MH (2022) Restormer: Efficient transformer for high-resolution image restoration. In: Proceedings of the IEEE/CVF conference on computer vision and pattern recognition, pp 5728–5739

Zeng H, Wang X, Chen Y, Su J, Liu J (2025) Vision-language gradient descent-driven all-in-one deep unfolding networks. In: Proceedings of the Computer Vision and Pattern Recognition Conference, pp 7524–7533

Zhang H, Patel VM (2018) Densely connected pyramid dehazing network. In: Proceedings of the IEEE conference on computer vision and pattern recognition, pp 3194–3203

Zhang J, Cao Y, Wang Z (2014) Nighttime haze removal based on a new imaging model. In: 2014 IEEE international conference on image processing (ICIP), IEEE, pp 4557–4561

Zhang J, Cao Y, Fang S, Kang Y, Wen Chen C (2017) Fast haze removal for nighttime image using maximum reflectance prior. In: Proceedings of the IEEE conference on computer vision and pattern recognition, pp 7418–7426

Zhang J, Cao Y, Zha ZJ, Tao D (2020) Nighttime dehazing with a synthetic benchmark. In: Proceedings of the 28th ACM international conference on multimedia, pp 2355–2363

Zhang R, Isola P, Efros AA, Shechtman E, Wang O (2018) The unreasonable effectiveness of deep features as a perceptual metric. In: Proceedings of

the IEEE conference on computer vision and pattern recognition, pp 586–595

Zhang S, Ren W, Tan X, Wang ZJ, Liu Y, Zhang J, Zhang X, Cao X (2021) Semantic-aware dehazing network with adaptive feature fusion. *IEEE Transactions on Cybernetics* 53(1):454–467

Zhang X, Ma J, Wang G, Zhang Q, Zhang H, Zhang L (2025) Perceive-IR: Learning to perceive degradation better for all-in-one image restoration. *IEEE Transactions on Image Processing*

Zhang Y, Zhou S, Li H (2024) Depth information assisted collaborative mutual promotion network for single image dehazing. In: *Proceedings of the IEEE/CVF Conference on Computer Vision and Pattern Recognition*, pp 2846–2855

Zhao X (2021) Single image dehazing using bounded channel difference prior. In: *Proceedings of the IEEE/CVF conference on computer vision and pattern recognition*, pp 727–735

Zhao Z, Yan J, Li C, Wang X, Tang J (2025) DehazeMamba: Sar-guided optical remote sensing image dehazing with adaptive state space model. *arXiv preprint arXiv:250313073*

Zheng Y, Zhan J, He S, Dong J, Du Y (2023) Curricular contrastive regularization for physics-aware single image dehazing. In: *Proceedings of the IEEE/CVF conference on computer vision and pattern recognition*, pp 5785–5794

Zhu JY, Park T, Isola P, Efros AA (2017) Unpaired image-to-image translation using cycle-consistent adversarial networks. In: *Proceedings of the IEEE international conference on computer vision*, pp 2223–2232

Zhu Q, Mai J, Shao L (2015) A fast single image haze removal algorithm using color attenuation prior. *IEEE transactions on image processing* 24(11):3522–3533